Main Manuscript for

Succinate is Broadly Tissue-Permeant and Uncouples Mitochondrial Respiration from ATP Synthesis

Daniel T. Hass[1], Brian M. Robbings[1,2], Celia M. Bisbach[1], Elizabeth Giering[3], Thomas O. Mundinger[3], Martin Sadilek[4], Ian R. Sweet[2], James B. Hurley[1*]

[1]*Biochemistry Department, The University of Washington, Seattle WA 98109*
[2]*Diabetes Institute, The University of Washington, Seattle WA 98109*
[3]*Division of Endocrinology/Metabolism, Veterans Affairs Puget Sound Health Care System, Seattle, WA*
[4]*Chemistry Department, The University of Washington, Seattle WA 98109*
*Corresponding Author

Email: jbhhh@uw.edu

Author Contributions: DTH, CMB, and JBH conceived of the project, which was supervised by JBH. DTH, BMR, CMB, EG, and TM performed the experiments. BMR, EG, TM, MS, and IRS provided critical methodological support. DTH and BMR analyzed the experiments. JBH and IRS provided reagents. DTH, CMB, and JBH secured the funding. DTH wrote the original draft of the manuscript, which was reviewed and edited by all authors.

Competing Interest Statement: The authors declare no competing interests.

Classification: Biological Sciences, Biochemistry

Keywords: Succinate, Eye, Uncoupling, Mitochondria, ^{13}C-Infusion

This PDF file includes:

Main Text
Figures 1 to 5
Tables 1 to 2

Abstract

Succinate is present in circulation and its concentration is influenced by hypoxic stress. Transporters have been identified that can facilitate import of succinate, yet previous reports suggest that most cells do not take up succinate from the blood. We directly tested the hypothesis that succinate is imported from the blood in vivo and metabolized. We infused ^{13}C-succinate into mice and followed its incorporation into metabolic intermediates into tissues. We also used respirometry to evaluate the abilities of isolated tissues to oxidize succinate. Most tissues take up and oxidize succinate following a bolus infusion. Retina tissue has the most unique and unexpected response to succinate. By tracing ^{13}C from the infused succinate, we found that the retina utilizes carbons from succinate in gluconeogenesis. In eyecup preparations including retinal pigment epithelium, a monolayer of cells directly adjacent to the retina *in situ*, succinate stimulates mitochondrial uncoupling. Our data reveal broad utilization of succinate and unique tissue-specific metabolic roles for it.

Significance Statement

Succinate fuels energy metabolism but was thought to be both created and consumed exclusively in mitochondria. Blood succinate increases with diabetes, exercise, and hypoxia, yet how this is connected to mitochondria remains unknown. We use multiple techniques to show that succinate supplied outside tissues is taken up and consumed by the mitochondria of those tissues. Unlike other tissues the retina is unique in its capability to fuel gluconeogenesis using succinate. At high concentrations, succinate also uncouples mitochondrial respiration independently of most known mechanisms of uncoupling. Together our data show that there is much to learn regarding the biology of this molecule alongside its classical role in the electron transport chain.

Main Text

Introduction

Succinate is a key intermediate in the Krebs cycle in the mitochondrial matrix where it provides reducing power to the electron transport chain (ETC). Electrons from succinate reduce coenzyme Q_{10} (QH_2) and the subsequent flow of electrons from QH_2 to O_2 via ETC complexes generates a proton motive force (Δρ) across the inner mitochondrial membrane. Δρ powers ATP synthesis and transport of P_i, pyruvate, glutamate, and adenine nucleotides into the mitochondrial matrix (Gutiérrez-Aguilar & Baines, 2013).

Succinate also is present in blood at concentrations from 0-50 μM, though this may increase to 150 μM with obesity or exercise, or 200 μM with type-2 diabetes (Hochachka & Dressendorfer, 1976; Kushnir et al., 2001; Serena et al., 2018). Restricted access to O_2 also increases circulating succinate concentrations to 174 μM in hypertensive rodents euthanized with CO_2 (Sadagopan et al., 2007) and in excess of 300 μM when seals are forced to dive and become hypoxic (Hochachka et al., 1975). Succinate in blood originates from muscle (Hochachka & Dressendorfer, 1976), pancreas (Jang et al., 2019), and possibly from gut microbiota (Serena et al., 2018). The relative contributions of these and other sources to circulating succinate has not been established. The metabolic impact and the fate of circulating succinate also are not known.

Brown adipose tissue can use succinate from the blood to fuel thermogenesis (Mills et al., 2018). We recently found that extracellular succinate also increases respiration in *ex vivo* eyecup tissue (consisting of sclera, choroid, and retinal pigment epithelium) (Bisbach et al., 2020). However, several reports have suggested that exogenous succinate is not imported into most other types of cell (Clerc & Polster, 2012; Ehinger et al., 2016; MacDonald et al., 1989; Protti, 2018). Nevertheless, monocarboxylate and dicarboxylate transporters that can transport succinate are expressed in many tissues (Andrienko et al., 2017; Nakai et al., 2006; Pajor, 2014; Prag et al., 2020; Reddy et al., 2020).

In this report we pursue ex vivo and in vivo strategies to establish which tissues take up and metabolize succinate. Consistent with our previous findings, succinate metabolism in the retina and eyecup are strikingly different. We also found that most tissues, including the eyecup, import and oxidize circulating and extracellular succinate. The retina occupies a unique niche however and utilizes succinate for gluconeogenesis.

Oxidation of succinate by mitochondria uncouples mitochondrial respiration from ATP synthesis. Uncoupling is not associated with oxidative stress, adenine nucleotide transporter activity, or the mitochondrial permeability transition pore complex. Our findings suggest that extracellular succinate is used as a fuel by most cells and it is capable of directly uncoupling mitochondria through mitochondrial membrane potential-dependent increases in H^+-leak. Because the retina normally produces succinate this may mean that mitochondrial uncoupling plays a role in normal eyecup physiology.

Results

Extracellular Succinate Promotes O_2 Flux Ex Vivo

In the conventional Krebs cycle, succinate dehydrogenase oxidizes succinate to fumarate. The electrons from that reaction reduce coenzyme Q_{10}, cytochrome C, then O_2 (**Figure 1A**). Oxidation of succinate therefore stimulates O_2 consumption by complex IV. We used a perifusion respirometer to quantify O_2 consumption in isolated tissues that can be inhibited by KCN, a complex IV inhibitor. Figure 1B shows how the O_2 consumption rate (OCR) depends on succinate concentration. Increasing succinate concentrations (30 μM, 100 μM, 300 μM, 1 mM, 3 mM, 10 mM, 30 mM, and 100 mM all with 5 mM glucose present) stimulate the OCR of liver, cerebellum, interscapular brown adipose tissue (BAT), kidney, eyecup (containing retinal pigment epithelium, choroid, and sclera), and retina tissue. The data are fit with an allosteric sigmoidal function (**Figure 1C-H**). In most tissues, succinate enhances OCR with a best-fit V_{max} of 0.34-0.89 nmol O_2 / mg tissue / minute, and best-fit $K_{1/2}$ values ranged from 0.9-2.72 mM (**Table 1**), The retina lay far outside this range (V_{max} - 0.12 nmol O_2 / mg tissue / minute and $K_{1/2}$ estimated to be 8.9 mM). This succinate concentration-response curve for retina is an estimate because it did not reach saturation. This suggests either that in retinas there is unusually limited succinate transport or that the ETC of the retina has an unusually poor ability to oxidize succinate. In all other tissues we studied, succinate clearly stimulates mitochondrial respiration.

The effect of succinate on OCR could be mediated by SUCNR1, a G-protein coupled receptor that stimulates activity of genes involved in systemic metabolism (Prag et al., 2020; Wang et al., 2020). We attempted to stimulate this receptor in eyecup tissue using the SUCNR1 agonist cis-epoxysuccinate (500 μM). This concentration of agonist should be as potent for SUCNR1 as 5 mM succinate (Geubelle et al., 2017), yet in the presence of glucose it did not stimulate O_2 consumption (**Figure S1**), suggesting that the effects of succinate on OCR are not due to signaling through SUCNR1.

Infused Succinate is Metabolized In Vivo

Ex vivo experiments with tissue explants provide useful and important information, but the tissue isolation process may influence the integrity of the plasma membrane and mitochondria or the overall metabolic profile of a tissue. To address this concern we evaluated import of succinate into cells *in vivo* by infusing male and female C57BL6/J mice with a 100 mg/kg bolus of uniformly labeled (U)-^{13}C succinate dissolved in sterile saline (pH 7.4) through jugular vein catheters. Before infusion we withdrew two 10 μL baseline whole blood samples through a carotid catheter. Then we infused labeled succinate through the jugular catheter. We sampled 10 μL of blood at 0.5, 1, 2, 3, 4, 5, 7.5, and 10 minutes following the infusion and used gas chromatography–mass spectrometry (GC-MS) to measure the accumulation of ^{13}C on metabolites in glycolysis and the Krebs cycle (**Table 2**). Total blood U-^{13}C-succinate levels (as m+4 because it contains four ^{13}C atoms) spiked immediately following infusion and rapidly declined throughout the 10-minute

process (**Figure 2A**). A single exponential fit of m+4 succinate over time shows that infused succinate reached a half maximal concentration at 0.89 (95% CI: 0.6-1.31) minutes post-infusion. The dominant isotopologue in blood was m+4, showing that for at least 10 minutes following the bolus infusion, tissues have access to a pool of almost fully labeled succinate (**Figure 2B**). A molecule in blood spectrally overlaps with m+4 succinate and interferes with estimation of succinate isotopologue distribution in unlabeled blood samples. However, this signal contaminant contributes ~3.7% of the m+4 succinate signal 10 minutes following infusion, so it does not cause major errors in the isotopic correction algorithm in post-infusion blood samples. Following the infusion, m+4 labeling briefly appears in circulating fumarate and malate pools and is cleared by the time total m+4 succinate reaches a steady state in circulation (**Figure S2**).

We euthanized mice five minutes after the bolus infusion and used GC-MS to quantify tissue metabolites in the retina, cerebellum, eyecup, liver, lung, interscapular brown adipose tissue (BAT), and interscapular white adipose tissue (WAT). M+4 succinate was present in all tissues (**Figure 2C**), and in the retina m+4 succinate levels were significantly lower than in liver, lung, BAT, WAT, and blood. We estimated succinate turnover in these tissues from the fraction of succinate that is m+4. All tissues accumulated significantly less succinate pool labeling than blood. We compared succinate labeling in each tissue to the retina as a reference tissue that accumulates little succinate labeling. Fractional succinate labeling was significantly higher in eyecup, lung, BAT, and WAT than retina (**Figure 2D**). Fractional labeling reports the turnover of the pool in a tissue so it depends on overall succinate pool size. A low fractional labeling does not necessarily mean a tissue is not metabolizing succinate. We estimated succinate catabolism by summing the molar abundance of ^{13}C (originating from U-^{13}C-succinate) on all metabolites that we routinely measure (**Table 2**). We normalized this quantity to the molar abundance of ^{12}C in the same sample (**Figure 2E**). Compared to the retina, $^{13}C/^{12}C$ was significantly greater in eyecup, brown adipose tissue, and blood.

^{13}C from succinate labeled downstream intermediates in the conventional Krebs cycle. These include fumarate, malate, aspartate, citrate, and pyruvate. Enrichment of ^{13}C-label in these metabolites is a function of the amount of m+4 succinate present in each tissue (**Figure S3**). To compare how different tissues use succinate, we normalized the abundance of these labeled metabolites to m+4 succinate. **Figure 2F** shows the isotopologues expected to appear in tissues following conventional Krebs cycle-mediated succinate catabolism. 5-minutes post-infusion we find these labeled metabolites do accumulate, with relatively low labeling of downstream Krebs cycle intermediates in blood compared to within tissues (**Figure 2G-K**). All tissues accumulated significantly more m+4 fumarate/m+4 succinate than blood, and significantly less m+4 fumarate/m+4 succinate than eyecups. This implies that succinate oxidation may be faster in eyecup tissue than in others (**Figure 2G**). M+4 fumarate /m+4 succinate in retina was about the same as in other tissues (**Figure 2G**), suggesting that the poor response of retina OCR to succinate observed *ex vivo* reflects slower succinate import rather than oxidation. Higher m+4 fumarate in eyecups also leads to significantly more labeling relative to m+4 succinate in downstream intermediates such as malate (**Figure 2H**), citrate (**Figure 2I**), and aspartate (**Figure 2J**). These data suggest that SDH is more active in eyecups than other tissues. These tissue differences could be related to the abundance of mitochondrial content across different tissues. To evaluate, we performed immunoblots to determine the relative abundances of complex I, II, III, IV and V (ATP synthase) component proteins (NDUFS8, SDHB, UQCRC2, mt-CO1, and ATP5A). Levels of the Complex II component SDHB in eyecups are equal to or lower than in most other tested tissues. This suggests that m+4 fumarate labeling is not linked directly to expression of SDHB (**Figure S4**). While import of succinate into the retina is relatively slow, it does occur and can be detected by m+4 labeling of Krebs cycle intermediates. We reasoned that poor succinate import may be a sign that there are other differences in the way retina tissue handles m+4 succinate. We found that m+3 pyruvate/m+4 succinate was significantly higher in the retina than other tissues (**Figure 2K**), which may be indicative of substantial malic enzyme activity or PEPCK activity in the retina. Both of these are able to form m+3 pyruvate, either from m+4 malate → m+3 pyruvate, or from m+4 oxaloacetate → m+3 PEP → m+3 pyruvate.

Succinate Infusion Reveals Specialized Metabolic Features in the Retina and Eyecup

Succinate catabolism in the retina and eyecup followed distinct patterns. These tissues are adjacent in the eye, so we focused our investigation on succinate metabolism in these tissues. We followed ^{13}C flux 1, 2, 3, 5, and 12 minutes following infusion of 100 mg/kg U-^{13}C succinate. M+0 and m+4 succinate are the principal isotopologues following infusion. These species decay following the bolus infusion as ^{13}C-succinate carbons flow into different metabolic pathways. This decay suggests that in the 11 minutes following infusion, ~44% of the eyecup succinate pool is m+4 labeled then replaced by unlabeled succinate (**Figure 3A**) Only ~5% of the succinate pool is m+4 labeled then replaced in retinas (**Figure 3B**). As a consequence of higher m+4 succinate turnover in eyecups, downstream m+4 or m+3 isotopologues of malate (**Figure 3D**), aspartate (**Figure 3G**), citrate (**Figure 3J**), α-ketoglutarate (**Figure 3M**), isocitrate (**Figure S5A**), and glutamate **(Figure S5D)** accumulate more rapidly in eyecup than in retina, showing that the conventional Krebs cycle is highly active in this tissue. Lesser ^{13}C-succinate import to the retina yields lower fractional ^{13}C labeling in downstream intermediates such as malate and citrate (**Figure 3E,K**).

Poor ^{13}C labeling also may be influenced by alternate metabolic pathways that could lead to different metabolic endpoints. The absence of m+4 aspartate or citrate in the retina suggested that oxaloacetate is diverted away from reactions that form citrate or aspartate, or that oxaloacetate does indeed become citrate, but the citrate pool is very large in comparison to the malate pool and dilutes the m+4 label. However, our analysis showed that the retina citrate pool is not larger than the malate pool, so we investigated alternate metabolic pathways for malate carbons (**Figure 3**). We followed ^{13}C labeling on glycolytic intermediates and found that m+3 PEP/ m+4 succinate is highest in retina and eyecup tissue compared to all the other tissues (**Figure 4A**). A closer investigation revealed that m+3 pyruvate, phosphoenolpyruvate (PEP), and 3-phosphoglycerate (3PG) accumulates over time in retina and eyecup tissue (**Figure 4C-K**). Accumulation of ^{13}C from succinate on these intermediates suggests gluconeogenic activity, most likely due to activity of the enzyme phosphoenolpyruvate carboxykinase (*PEPCK),* which catalyzes decarboxylation of oxaloacetate (m+4 labeled if its carbons originated as infused succinate) to form m+3 phosphoenolpyruvate and m+1 CO_2. The PEP can become m+3 3PG through the reversible steps of glycolysis, or m+3 pyruvate through either pyruvate kinase or malic enzyme. M+3 3PG labeling occurs in both tissues, but the path leading to it is more active in retinas. In eyecups the succinate pool is more labeled but the 3PG pool is less labeled. This indicates that there is more gluconeogenic activity in the retina than in the eyecup. This gluconeogenic pathway (**Figure 4B**) requires that m+4 oxaloacetate be formed before becoming m+3 PEP. Our findings support this but they do not rule out a contribution of malic enzyme activity, to m+3 pyruvate formation. PEPCK activity is consistent with the time-dependent accumulation of m+1 labeling on α-ketoglutarate, isocitrate, citrate, and malate (**Figure 3**). Decarboxylation of m+4 oxaloacetate by PEPCK, m+3 pyruvate by PDH, m+4 isocitrate by isocitrate dehydrogenase, or m+4 α-ketoglutarate by α-ketoglutarate dehydrogenase generates m+1 CO_2, and pyruvate carboxylation can transfer this m+1 CO_2 to generate an m+1 labeled metabolite. Pyruvate carboxylase activity can form oxaloacetate from captured $^{13}CO_2$.

It is important to consider that retinas are made up of several distinct types of neurons and glia. We detected very little m+4 citrate in the retina (**Figure 3K**), suggesting limited ^{13}C succinate use by the Krebs cycle. Instead of accumulating m+4 intermediates, the retina Krebs cycle accumulates m+2 intermediates. The most likely source of these is m+3 pyruvate, which is used by pyruvate dehydrogenase to form m+2 acetyl-CoA and downstream m+2 intermediates. This means that retina m+2 citrate is likely to made by the condensation of m+2 acetyl-CoA and unlabeled oxaloacetate. M+3 PEP formation from PEPCK requires m+4 oxaloacetate, and yet if there is m+4 oxaloacetate available to make m+3 PEP, that m+4 oxaloacetate should also be available to make m+4 or m+6 citrate. We do not find substantial accumulation of m+4 or m+6 citrate, suggesting that within the retina, production of m+3 PEP (from labeled oxaloacetate) and downstream m+2 citrate (from m+2 acetyl CoA and unlabeled oxaloacetate) occur in different

metabolic compartments, with unlabeled oxaloacetate originating from a compartment that does not take up m+4 succinate. The data that suggests gluconeogenic activity and consequent m+1 or m+2 labeling on Krebs cycle consistently appear in our analysis of *in vivo* ^{13}C-succinate flux. We tested whether these activities also occur in isolated tissues. We incubated explanted retinas and eyecups in 5 mM glucose + 50 μM U-^{13}C succinate for 0, 0.5, 1, 2, and 5 minutes. The tissues were metabolically active and imported the labeled succinate, yet they did not form m+3 3-PG, suggesting that the factors enable gluconeogenesis *in vivo* are not recapitulated in our *ex vivo* culture system (**Figure S6**).

Succinate Stimulates Mitochondrial Uncoupling in Eyecup Tissue Isotopologues

Our analyses of ^{13}C succinate flux *in vivo* suggests gluconeogenic activity in the retina and oxidation of succinate in the eyecup (**Figures 1G, 2D, 2E, and 3**). The extent to which increasing concentrations of succinate stimulate mitochondrial O_2 consumption (**Figure 1**) is surprising, as the capacity of tissues to oxidize mitochondrial substrates is limited by the mitochondrial proton motive force (Δρ). Substrate oxidation increases Δρ, which inhibits further substrate oxidation. We validated this with the conventional mitochondrial substrate pair pyruvate/malate. By increasing the concentration of these substrates and measuring eyecup OCR, we showed that these O_2 consumption fueled by NADH-linked substrates is limited and becomes maximal at ~3 mM pyruvate + 3 mM malate (**Figure 5A**).

Succinate oxidation also increases OCR, but eyecup succinate oxidation reaches its V_{max} at a higher substrate concentration (~30 mM, **Figure 1**). However, succinate and NADH promote different levels of mitochondrial H^+ flux per O_2 molecule. We converted substrate-dependent OCR (**Figure 5A**) into estimates of H^+ flux, assuming (**1**) all OCR above the 5 mM glucose 'baseline' is from oxidation of the supplied substrate, and (**2**) each O_2 molecule consumed using NADH linked substrates catalyzed translocation of 10 $H^+/2e^-$ while succinate-dependent OCR translocated to an $H^+/2e^-$ ratio of 6 (**Figure 5B**). The effect of succinate and pyruvate/malate concentration on H^+ translocation overlapped at 300 μM and lower but deviated at ≥1 mM, with higher succinate concentrations inducing a greater H^+ flux than equimolar pyruvate/malate. The mismatch in OCR/H^+ flux suggests that exogenous succinate produces a H^+ leak across the inner mitochondrial membrane that is compensated for by additional substrate oxidation. We determined whether succinate produces H^+ leak by exposing eyecup tissue to either 5 mM succinate or 5 mM pyruvate/malate in the presence of the ATP synthase inhibitor oligomycin. O_2 consumption in the presence of oligomycin represents substrate oxidation that is not inhibited by Δρ. Leak respiration occurs at 5 mM of either substrate but is significantly greater with succinate than pyruvate/malate (**Figure 5C**).

We determined the extent to which succinate stimulates oligomycin-insensitive OCR by titrating succinate in the presence of oligomycin (**Figure 5D**). Succinate increases leak respiration at concentrations ≥ 300 μM. Multiple mechanisms could drive succinate dependent H^+ leak, including reactive oxygen species-induced activation of an uncoupling protein (Echtay et al., 2002; Mills et al., 2018), activation of H^+ leak through the adenine nucleotide translocase (ANT) (Bertholet et al., 2019), or activation of the mitochondrial permeability transition pore complex (mPTP) (Novgorodov et al., 1992). We stimulated succinate dependent H^+ leak by exposing eyecup tissue to 5 mM glucose, 10 μM oligomycin, and 5 mM succinate, and attempted to prevent succinate-stimulated leak respiration using inhibitors of oxidative stress (50 μM mitoTempo, 100 μM n-propyl gallate; **Figure 5E**), the ANT (30 μM carboxyatractyloside; **Figure 5F**), or the mPTP complex (2 μM cyclosporine A; **Figure 5G**). None of these compounds suppressed succinate-dependent leak respiration. We also tested whether succinate-dependent leak respiration occurs due to reverse complex I activity, which could oxidize coenzyme Q_{10}, reduce NAD^+, and transport H^+ from the mitochondrial intermembrane space to the matrix. The complex I Q-site inhibitor rotenone partially suppressed leak respiration (**Figure 5H**). We initially considered this to be a consequence of inhibiting complex I reversal fueled by succinate-dependent reduction of the coenzyme Q_{10} pool. However, the effect of rotenone also could be explained by cutting off the supply of electrons from glucose-derived NADH that can fuel OCR.

We evaluated the contribution of glucose to OCR by removing it from the medium. Glucose removal partially suppressed OCR and prevented rotenone from affecting OCR (**Figure 5I**). That indicates that the effect of succinate on H^+ leak is not caused by reversal of proton pumping through complex I.

Discussion

Extracellular Succinate is Utilized Ex Vivo and In Vivo

Mitochondrial succinate produced within the Krebs cycle can fuel respiration. We find that succinate also can fuel respiration when delivered extracellularly to intact tissues (**Figure 1**). Succinate stimulates O_2 consumption by isolated tissues with a half-maximal effect between 0.9 and 2.7 mM in all tissues except retina (**Table 1**). Tissues also take up and metabolize succinate *in vivo*. Shortly after ^{13}C-succinate is infused into the blood of freely moving mice it is taken up into tissues and oxidized in the Krebs cycle This suggests that under conditions where steady state circulating succinate concentration increase (exercise, diabetes, or hypoxia), succinate production may outpace the capacity for rapid uptake. (**Figure 2**).

We quantified succinate pool turnover (**Figure 2D**) and labeling of downstream metabolites with ^{13}C relative to ^{12}C (**Figure 2E**). These metrics show that succinate is oxidized to the greatest extent in eyecup, lung, and BAT. The ^{13}C-labeling metrics may underestimate succinate oxidation in eyecup, as the RPE may also import unlabeled succinate produced by the retina (Bisbach et al., 2020). Eyecup and lung tissue have high vascular access that may explain why m+4 succinate populates these pools so quickly. In BAT other mechanisms may contribute to rapid succinate utilization. For example, basal uncoupling could accelerate Krebs cycle activity so that succinate is oxidized quickly to fuel thermogenesis (Mills et al., 2018).

The retina responds to succinate differently than other tissues. Ex vivo, succinate only slightly stimulates OCR (**Figure 1H**) and compared to other tissues retina takes up less ^{13}C-succinate (**Figure 2C-E**). Retina tissue explants export succinate (Bisbach et al., 2020), and this export process may limit import. Overall, the retina appears to favor synthesis and export of succinate over import and oxidation.

We provide evidence that many tissues can take up and oxidize circulating succinate. This is consistent with a report that succinate stimulates consumption of O_2 by explants of dog heart and rabbit kidney (Furchgott & Shorr, 1948). However, our findings differ from reports that succinate does not stimulate O_2 consumption by cultured cells (Ehinger et al., 2016; MacDonald et al., 1989; Mills et al., 2018). Long-term cell culture can alter expression of metabolite transporters (Hanu et al., 2000). Diminished expression of succinate transporters could explain the differences between the metabolic responses of cultured cells compared to tissues. Testing this hypothesis will require identifying the proteins that transport succinate into tissues.

Evidence of Gluconeogenesis In Ocular Tissues

Surprisingly, ^{13}C from U-^{13}C-succinate imported *in vivo* into retinas labels PEP and 3PG (**Figure 2K, 4**). This suggests that oxaloacetate derived from ^{13}C-succinate is used by PEPCK and reversible glycolytic enzymes to makem+3 PEP and 3-PG through the activities of PEPCK and reversible glycolytic enzymes. We also noted that Krebs cycle intermediates become labeled with one ^{13}C (m+1, **Figure 3**) . Pyruvate carboxylase (PC) can use $^{13}CO_2$ released by oxidative decarboxylation of Krebs cycle intermediates to make m+1 oxaloacetate. PEPCK and PC activities are both evidence of gluconeogenesis. The portion of ^{13}C that enters the path to gluconeogenesis is more substantial in retina than in eyecups (**Figure 4**). This process occurs predominantly *in vivo* (**Figure S6**). We were concerned that that m+3 labeled glycolytic intermediates could be derived from ^{13}C labeled glucose made by gluconeogenesis in the liver.

However, the livers of infused mice had no detectable m+3 gluconeogenic intermediates in these experiments (**Figure 4A**).

Extracellular Succinate Uncouples Mitochondria

Succinate oxidation and downstream Krebs cycle activity are rapid in eyecups (**Figure 2**). That is surprising because succinate-dependent electron flux through complexes III and IV increase the proton-motive force(Δρ). A high Δρ generally limits respiration because transport of electrons to O_2 is coupled directly to H^+ pumping. Oligomycin blocks mitochondrial matrix H^+ influx through ATP synthase. Normally oligomycin causes Δρ to build to the point where NADH oxidation by complex I and O_2 reduction by complex IV are unfavorable (State 4, (Brand & Nicholls, 2011; Chance & Williams, 1955)).

Oligomycin blocks glucose-stimulated respiration in eyecup tissue as expected. However, we found that succinate overcomes the effect of oligomycin. H^+ leakage can partially relieve the effect of oligomycin on electron transport. The ability of succinate to overcome the effect of oligomycin suggests that succinate may partially dissipate Δρ. NADH-linked substrates pyruvate and malate do not have the same effect as succinate, suggesting that the apparent H^+ leak is unique to the biochemistry of succinate (**Figure 5A-B**). We titrated succinate in the presence of oligomycin and found that even low concentrations of extracellular succinate (<100 μM) can fuel leak respiration in the presence of oligomycin (also known as mitochondrial uncoupling).

This uncoupling effect of succinate could reflect either oxidative stress-stimulated uncoupling protein activity (Echtay et al., 2002; Mills et al., 2018), adenine nucleotide translocator (ANT) activity (Bertholet et al., 2019), or mitochondrial permeability transition pore complex activity. We used the antioxidants mitoTempo and n-propyl gallate to inhibit oxidative damage, cyclosporine A to inhibit the mPTP, and carboxyatractyloside to inhibit ANT activity. None of them alters oligomycin resistant succinate-stimulated OCR (**Figure 5E-G**). Only rotenone partially inhibits succinate-stimulated, oligomycin-resistant OCR (**Figure 5H**). Rotenone diminishes the reducing power from glucose-derived NADH (**Figure 5I**). These findings show that oligomycin stops complex I-driven OCR, and that this block can be overcome by succinate.

While we focus on eyecup tissue in this study, previous reports have demonstrated an exponential relationship between Δρ and H^+ leak in isolated mitochondria, particularly when the mitochondrial membrane is hyperpolarized (Brown & Brand, 1986; Nicholls, 1974). Increasing succinate flux increases the polarity of the mitochondrial membrane, and consequently, H^+ leak. Nicholls has proposed that Δρ-dependent dielectric breakdown of the mitochondrial membrane causes this H^+ leak (Nicholls, 1974). This mechanism of action for succinate is difficult to test conclusively in tissue. Follow-up investigations of our findings should focus on developing new strategies to identify the molecular and biophysical mechanism of succinate-induced uncoupling.

Succinate-induced mitochondrial uncoupling can occur in intact tissue *ex vivo* (**Figure 5**) or *in vitro* (Mills et al., 2018), but further studies will be needed to show that it also occurs *in vivo*. The concentration of circulating succinate reaches up to 150 μM with obesity and 200 μM with type-2-diabetes (Serena et al., 2018), 150 μM during exercise in humans (Hochachka & Dressendorfer, 1976), and in excess of 300 μM when seals are forced to dive and become hypoxic (Hochachka et al., 1975). Most tissues are therefore not normally exposed to the millimolar succinate concentrations that elicit the most substantial effects on OCR. However, we found that succinate at concentrations as low as 100 mM can stimulate uncoupled respiration. Our findings suggest that succinate released from the retina (Bisbach et al., 2020) could fill the limited volume of the subretinal space with sufficient succinate to stimulate mitochondrial uncoupling in eyecup tissue under physiological conditions.

Materials and Methods

Ethical Approval

This study was carried out in accordance with the National Research Council's Guide for the Care and Use of Laboratory Animals (*8th ed*). All protocols were approved by the Institutional Animal Care and Use Committees at the University of Washington and the VA Puget Sound Hospital.

Animals

In all experiments, we used 2-5 month-old wild-type C57BL6/J mice. These mice were housed at an ambient temperature of 25°C, with a 12-hour light cycle and *ad libitum* access to water and normal rodent chow.

Small animal surgeries

The procedure for chronic jugular vein and carotid artery catheterization was performed as previously described (Ayala et al., 2011) by the Cell Function and Analysis Core of the University of Washington's Diabetes Research Center. Briefly, following induction and maintenance under systemic inhaled anesthesia (isoflurane 1.5-2% in 1L/min), mice were administered with 4 mg/kg ketoprofen to reduce post-surgical swelling and provide analgesia. For intravenous infusions, jugular veins were isolated through a lateral incision to the trachea, and a silastic catheter was introduced into the vein, anchored to surrounding tissue, tunneled subcutaneously to the nape of the neck and connected to a vascular access port. A subset of mice received a contralateral carotid artery cannulation for blood sampling. The catheters were filled with heparinized saline, the skin incisions were sutured, and the mice recovered for 1 week before conscious infusion studies.

In vivo infusions

Jugular vein infusion studies were performed on freely moving, chronically cannulated mice. This system allowed us to avoid the potential confounding effects of acute surgical stress (Walters et al., 1992) or anesthesia (Windeløv et al., 2016) on succinate uptake or metabolism. We infused 100 mg/kg U-^{13}C-succinate (Cambridge Isotopes, CLM-1571) through jugular catheters over a period of approximately 20 seconds and euthanized awake mice by cervical dislocation 1, 2, 3, 5, or 10 minutes following the infusion. When mice possessed both carotid artery and jugular vein catheters, we took two 10 µL baseline blood samples per mouse then infused 100 mg/kg U-^{13}C-succinate through the jugular catheter. We sampled 10 µL of blood 0.5, 1, 2, 3, 4, 5, 7.5, and 10 minutes following the infusion, then euthanized mice. Following euthanasia we quickly dissected retinas and eyecups (a complex of the retinal pigment epithelium, sclera, and choroid vasculature) from the eye. For the 5 minutes post-infusion time point, we also dissected liver, lung, cerebellum, interscapular white adipose tissue, and interscapular brown adipose tissue. Dissected tissues were snap frozen in liquid N_2. All mice were euthanized between 10 AM and 1 PM to minimize circadian effects on metabolic function.

Ex vivo metabolic flux

In all *ex vivo* labeling experiments, we quickly euthanized mice by awake cervical dislocation, dissected the indicated tissues in Hank's Buffered Salt Solution (HBSS; GIBCO, Cat#: 14025-076), and incubated them in pH 7.4 Krebs-Ringer bicarbonate (KRB) buffer (98.5 mM NaCl, 4.9 mM KCl, 1.2 mM KH_2PO_4 1.2 mM $MgSO_4$-$7H_2O$, 20 mM HEPES, 2.6 mM $CaCl_2$-$2H_2O$, 25.9 mM $NaHCO_3$) supplemented with 5 mM glucose and [U-^{13}C]-succinic acid (Cambridge isotope CLM-1571-0.1; concentrations indicated in figures). This buffer was pre-equilibrated at 37°C, 21% O_2, and 5% CO_2 prior to incubations. Following incubations, tissue was flash frozen in liquid N_2.

Metabolite Extraction

Metabolites were extracted using 80% MeOH, 20% H_2O supplemented with 10 μM methylsuccinate (Sigma, M81209) as an internal standard to adjust for any metabolite loss during the extraction and derivatization procedures. The extraction buffer was equilibrated on dry ice, and 150 μL was added to each sample. Tissues were then disrupted by sonication and incubated on dry ice for 45 minutes to precipitate protein. Proteins were pelleted at 17,000 x g for 30 minutes at 4°C. The supernatant containing metabolites was lyophilized at room-temperature until dry and stored at -80°C until derivatization. The pellet containing protein was resuspended by sonication in RIPA buffer (150 mM NaCl, 1.0% Triton X-100, 0.5% sodium deoxycholate, 0.1% SDS, 50 mM Tris, pH 8.0) and the amount of protein was determined by a BCA assay (ThermoFisher, 23225).

Metabolite Derivatization

Lyophilized samples were first derivatized in 10 μL of 20 mg/mL methoxyamine HCl (Sigma, Cat#: 226904) dissolved in pyridine (Sigma, Cat#: 270970) at 37°C for 90 minutes, and subsequently with 10 μL tert-butyldimethylsilyl-N-methyltrifluoroacetamide (Sigma, Cat#: 394882) at 70°C for 60 minutes.

Gas Chromatography-Mass Spectrometry

Metabolites were analyzed on an Agilent 7890/5975C GC-MS using selected-ion monitoring methods described extensively in previous work (Du et al., 2015). Peaks were integrated in MSD ChemStation (Agilent), and correction for natural isotope abundance was performed using the software IsoCor (Millard et al., 2019). Corrected metabolite signals were converted to molar amounts by comparing metabolite peak abundances in samples with those in a ‘standard mix’ containing known quantities of metabolites we routinely measure. Multiple concentrations of this mix were extracted, derivatized, and run alongside samples in each experiment. These known metabolite concentrations were used to generate a standard curve which allowed for metabolite quantification. Metabolite abundance was normalized to tissue protein concentration, and following this, paired tissues such as retinas and eyecups from the same mouse were treated as technical replicates and averaged.

Ex vivo oxygen consumption

Following euthanasia, mouse tissues were dissected and cut into small segments in Hank's buffered salt solution. These tissues were incubated in Krebs-Ringer bicarbonate buffer (KRB) supplemented with 5 mM glucose and pre-equilibrated at 37°C and 5% CO_2. We determined OCR using a custom-built perifusion flow-culture system (Neal et al., 2015; Sweet et al., 2002). Tissues were perifused in chambers between Cytopore beads (Amersham Biosciences, Piscatawy, NJ) and porous frits. With KRB supplemented with 5 mM glucose, 1x Antibiotic-Antimycotic (Gibco), and 1 mg/mL fatty acid-free bovine serum albumin. An artificial lung oxygenated supplemented KRB with a mixture of 21% O_2, 5% CO_2, and 74% N_2.Oxygenated media was passed through a bubble trap before exposure to mouse tissues. Outflow media came into contact with a glass wall coated with a thin layer of oxygen sensitive polymerized Pt(II) Meso-tetra(pentafluorophenyl)porphine dye (Frontier Scientific, Logan, UT) painted on the inner glass wall of the chamber. Following a 405 nm light pulse, the dye-coated glass emits a phosphorescent signal detected at 650 nm. The decay lifetime is dependent on oxygen tension. The flow rate of KRB along with the quantitative relationship between dye phosphorescent decay and oxygen concentration were used to determine tissue OCR. All OCR measurements were obtained under control conditions (baseline, 5 mM glucose), one or more experimental conditions, and a ‘zeroed’ condition wherein 3 mM potassium cyanide (KCN) was used to directly inhibit complex IV and thus subtract the effect of residual non-mitochondrial oxygen consumption from our measurements.

Western Blot

Protein was extracted by sonication in RIPA buffer supplemented with a protease and phosphatase inhibitor cocktails (ThermoFisher, Cat#: 78442). SDS sample buffer was added and samples were run on 13% polyacrylamide gels. After running, gels were transferred onto PVDF membranes (Millipore, IPFL00010) and rinsed with PBS. Primary antibody (anti-Total Oxphos, 1:1000 dilution, RRID: AB_2629281, Lot# P3338) was diluted in blocking buffer (LI-COR, 927–40,000) and incubated overnight on blots at 4°C. Membranes were washed twice with PBS containing 0.1% Tween-20 and once with PBS, then incubated with secondary antibody (IRDye 800CW goat anti-mouse IgG (H + L) (LI- COR Biosciences, 925-32210, RRID: AB_2687825) at 1:5000 in blocking buffer for 1 h at RT and washed again before imaging. Membranes were imaged and bands were quantified using the LI-COR Odyssey CLx Imaging System (RRID:SCR_014579).

Statistical Analysis

We performed all statistical data analyses using Prism Version 8 (GraphPad Software). The significance threshold was set at $p<0.05$. In all figures, *$p<0.05$, **$p<0.01$, ***$p<0.001$, and ****$p<0.0001$. *(Figure 1)* To fit curves of oxygen consumption as a function of [succinate], for each sample we averaged steady-state oxygen consumption over >5 minutes at the end of a given treatment. These averaged values were considered to be the OCR at each given [succinate] for each sample. We fit the curve to an allosteric sigmoidal shape in order to obtain approximations of V_{max}, $K_{1/2}$, and Hill's coefficient (h) (Table 1). *(Figure 2)* We estimated the half-life of infused m+4 succinate in blood by a one-phase decay function to the data. The abundance (*Figure* 2C), fractional labeling (*Figure* 2D), and ratios of metabolite isotopologues (*Figure 2E*) were compared using a one-way ANOVA. *(Figure 5)* We analyzed differences in respiration following treatments using one-way ANOVAs . The values input into these ANOVAs are averaged steady-state oxygen consumption over >5 minutes at the end of a given treatment.

Acknowledgments

The authors thank Susan Brockerhoff, Ph.D. and Michelle Giarmarco, Ph.D. for their help in editing this manuscript. This research was supported by funding from the following sources T32 EY007031/EY/NEI NIH HHS/United States (to DTH), F31 EY031165/EY/NEI NIH HHS/United States (to CMB), R01 EY006641/EY/NEI NIH HHS/United States (to JBH), R01 EY017863/EY/NEI NIH HHS/United States (to JBH). OCR studies and conscious jugular infusion studies were performed at the Cell Function Analysis Core of the Univ. of Washington's Diabetes Research Center, which is supported by P30 DK017047/DK/NIDDK NIH HHS/United States.

References

1. M. Gutiérrez-Aguilar, C. P. Baines, Physiological and pathological roles of mitochondrial SLC25 carriers. *Biochem J* **454**, 371-386 (2013).
2. P. W. Hochachka, R. H. Dressendorfer, Succinate accumulation in man during exercise. *Eur J Appl Physiol Occup Physiol* **35**, 235-242 (1976).
3. C. Serena *et al.*, Elevated circulating levels of succinate in human obesity are linked to specific gut microbiota. *ISME J* **12**, 1642-1657 (2018).
4. M. M. Kushnir, G. Komaromy-Hiller, B. Shushan, F. M. Urry, W. L. Roberts, Analysis of dicarboxylic acids by tandem mass spectrometry. High-throughput quantitative measurement of methylmalonic acid in serum, plasma, and urine. *Clin Chem* **47**, 1993-2002 (2001).
5. N. Sadagopan *et al.*, Circulating succinate is elevated in rodent models of hypertension and metabolic disease. *Am J Hypertens* **20**, 1209-1215 (2007).

6. P. W. Hochachka, T. G. Owen, J. F. Allen, G. C. Whittow, Multiple end products of anaerobiosis in diving vertebrates. *Comp Biochem Physiol B* **50**, 17-22 (1975).
7. C. Jang *et al.*, Metabolite Exchange between Mammalian Organs Quantified in Pigs. *Cell Metab* **30**, 594-606.e593 (2019).
8. E. L. Mills *et al.*, Accumulation of succinate controls activation of adipose tissue thermogenesis. *Nature* **560**, 102-106 (2018).
9. C. M. Bisbach *et al.*, Succinate Can Shuttle Reducing Power from the Hypoxic Retina to the O2 Rich Pigment Epithelium. *Cell Rep* **31**, 107606 (2020).
10. J. K. Ehinger *et al.*, Cell-permeable succinate prodrugs bypass mitochondrial complex I deficiency. *Nat Commun* **7**, 12317 (2016).
11. M. J. MacDonald, L. A. Fahien, R. J. Mertz, R. S. Rana, Effect of esters of succinic acid and other citric acid cycle intermediates on insulin release and inositol phosphate formation by pancreatic islets. *Arch Biochem Biophys* **269**, 400-406 (1989).
12. P. Clerc, B. M. Polster, Investigation of mitochondrial dysfunction by sequential microplate-based respiration measurements from intact and permeabilized neurons. *PLoS One* **7**, e34465 (2012).
13. A. Protti, Succinate and the shortcut to the cure of metformin-induced lactic acidosis. *Intensive Care Med Exp* **6**, 35 (2018).
14. H. A. Prag *et al.*, Mechanism of succinate efflux upon reperfusion of the ischemic heart. *Cardiovasc Res* (2020).
15. A. M. Pajor, Sodium-coupled dicarboxylate and citrate transporters from the SLC13 family. *Pflugers Arch* **466**, 119-130 (2014).
16. M. Nakai, L. Chen, R. A. Nowak, Tissue distribution of basigin and monocarboxylate transporter 1 in the adult male mouse: a study using the wild-type and basigin gene knockout mice. *Anat Rec A Discov Mol Cell Evol Biol* **288**, 527-535 (2006).
17. T. N. Andrienko, P. Pasdois, G. C. Pereira, M. J. Ovens, A. P. Halestrap, The role of succinate and ROS in reperfusion injury - A critical appraisal. *J Mol Cell Cardiol* **110**, 1-14 (2017).
18. A. Reddy *et al.*, pH-Gated Succinate Secretion Regulates Muscle Remodeling in Response to Exercise. *Cell* **183**, 62-75.e17 (2020).
19. J. E. Ayala *et al.*, Hyperinsulinemic-euglycemic clamps in conscious, unrestrained mice. *J Vis Exp* (2011).
20. J. M. Walters, G. M. Ward, A. Kalfas, J. D. Best, F. P. Alford, The effect of epinephrine on glucose-mediated and insulin-mediated glucose disposal in insulin-dependent diabetes. *Metabolism* **41**, 671-677 (1992).
21. J. A. Windeløv, J. Pedersen, J. J. Holst, Use of anesthesia dramatically alters the oral glucose tolerance and insulin secretion in C57Bl/6 mice. *Physiol Rep* **4** (2016).
22. J. Du, J. D. Linton, J. B. Hurley, Probing Metabolism in the Intact Retina Using Stable Isotope Tracers. *Methods Enzymol* **561**, 149-170 (2015).
23. P. Millard *et al.*, IsoCor: isotope correction for high-resolution MS labeling experiments. *Bioinformatics* **35**, 4484-4487 (2019).
24. I. R. Sweet *et al.*, Dynamic perifusion to maintain and assess isolated pancreatic islets. *Diabetes Technol Ther* **4**, 67-76 (2002).
25. A. Neal *et al.*, Quantification of Low-Level Drug Effects Using Real-Time, in vitro Measurement of Oxygen Consumption Rate. *Toxicol Sci* **148**, 594-602 (2015).
26. T. Wang *et al.*, Succinate induces skeletal muscle fiber remodeling via SUCNR1 signaling. *EMBO Rep* **21**, e50461 (2020).
27. P. Geubelle *et al.*, Identification and pharmacological characterization of succinate receptor agonists. *Br J Pharmacol* **174**, 796-808 (2017).
28. K. S. Echtay *et al.*, Superoxide activates mitochondrial uncoupling proteins. *Nature* **415**, 96-99 (2002).
29. A. M. Bertholet *et al.*, H+ transport is an integral functi^{o}n of the mitochondrial ADP/ATP carrier. *Nature* **571**, 515-520 (2019).

30. S. A. Novgorodov, T. I. Gudz, Y. M. Milgrom, G. P. Brierley, The permeability transition in heart mitochondria is regulated synergistically by ADP and cyclosporin A. *J Biol Chem* **267**, 16274-16282 (1992).
31. R. F. Furchgott, E. Shorr, The effect of succinate on respiration and certain metabolic processes of mammalian tissues at low oxygen tensions in vitro. *J Biol Chem* **175**, 201-215 (1948).
32. R. Hanu, M. McKenna, A. O'Neill, W. G. Resneck, R. J. Bloch, Monocarboxylic acid transporters, MCT1 and MCT2, in cortical astrocytes in vitro and in vivo. *Am J Physiol Cell Physiol* **278**, C921-930 (2000).
33. M. D. Brand, D. G. Nicholls, Assessing mitochondrial dysfunction in cells. *Biochem J* **435**, 297-312 (2011).
34. B. Chance, G. R. Williams, Respiratory enzymes in oxidative phosphorylation. I. Kinetics of oxygen utilization. *J Biol Chem* **217**, 383-393 (1955).
35. D. G. Nicholls, The influence of respiration and ATP hydrolysis on the proton-electrochemical gradient across the inner membrane of rat-liver mitochondria as determined by ion distribution. *Eur J Biochem* **50**, 305-315 (1974).
36. G. C. Brown, M. D. Brand, Changes in permeability to protons and other cations at high proton motive force in rat liver mitochondria. *Biochem J* **234**, 75-81 (1986).

Figures and Tables

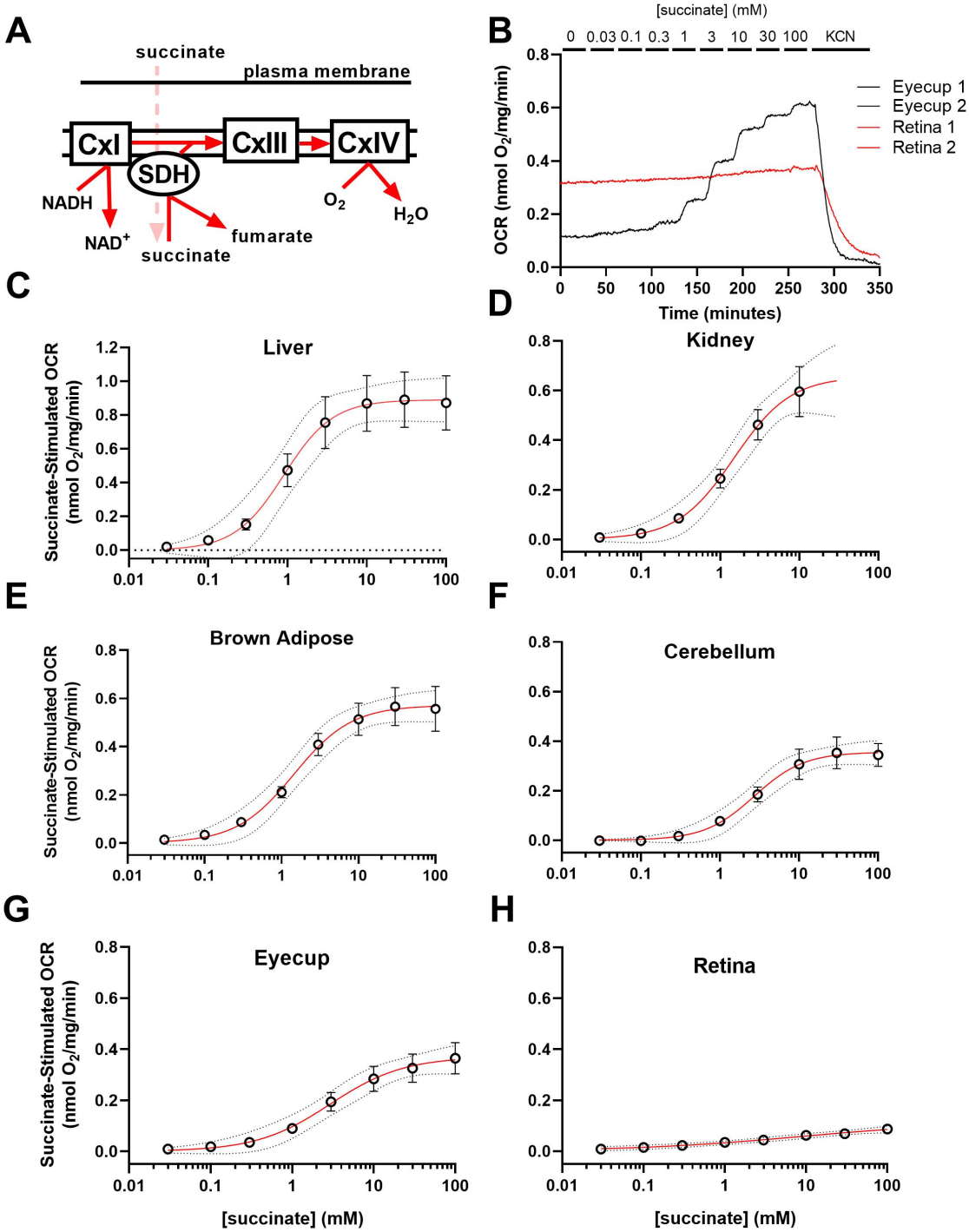

Figure 1. Extracellular Succinate Increases Oxygen Consumption in Diverse Tissues Ex Vivo. (**A**) Schematic of the mitochondrial electron transport chain, the main site of O_2 consumption in the mammalian cell. We measured O_2 consumption rate (OCR) in freshly dissected (**C**) liver (n=3), (**D**) kidney (n=4), (**E**) interscapular brown adipose (n=3)), (**F**) cerebellum (n=3), (**B,G**) eyecup (n=3), and (**B,H**) retina (n=4) tissue from C57BL6/J mice, perifused in

modified KRB buffer with 5 mM glucose as the principal metabolic fuel. We supplied this media with increasing concentrations of disodium succinate (30 μM, 100 μM, 300 μM, 1 mM, 3 mM, 10 mM, 30 mM, or 100 mM) and determined the consequent OCR above the 5 mM glucose "baseline" respiration. Examples of such experiments are shown in (**B**) with each line representing an individual sample. These data are summarized for different tissues in C-H as dots displaying mean steady-state OCR ± SEM. We estimated the dependence of OCR on [succinate] by fitting the data with an allosteric sigmoidal curve (red lines). Best-fit parameters are available in **Table 1**. Dotted lines surrounding the curves represent 95% confidence intervals from the curve fit.

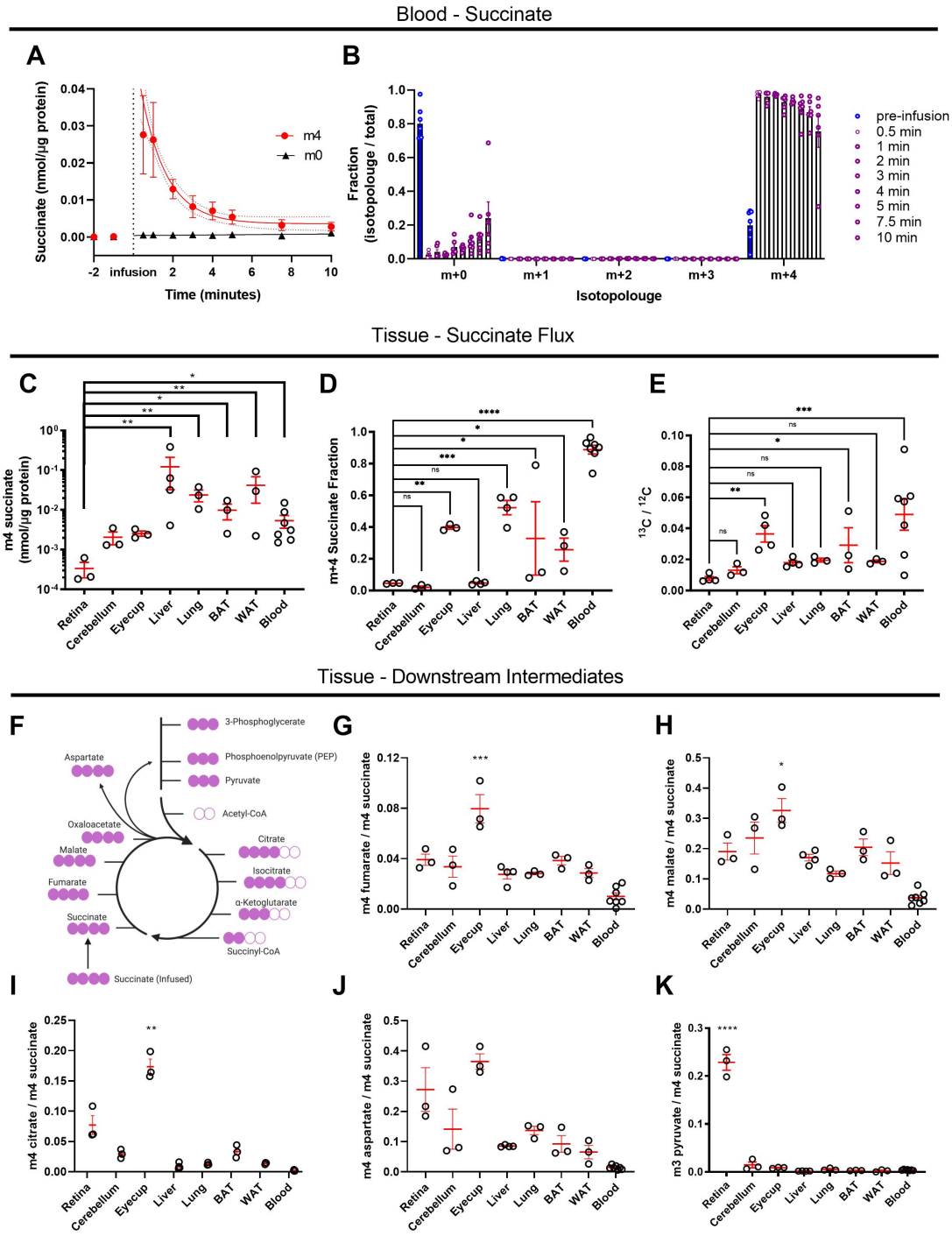

Figure 2. Systemic Metabolism of Infused Succinate. (**A-B**) We infused U-^{13}C-succinate into the mouse bloodstream and sampled blood 0.5 (n=5), 1 (n=5), 2 (n=7), 3 (n=6), 4 (n=5), 5 (n=7), 7.5 (n=6), and 10 (n=6) minutes post-infusion, with catheterized, un-infused mice as a "0 minute" control (n=7). **(A)** We measured unlabeled (m+0) and fully ^{13}C-labeled (m+4) succinate in blood post-infusion (plotted: mean ± SEM) and fit these data with a one-phase decay function (fit line ± 95% CI) **(B)** Isotopic abundance of blood succinate prior to (blue) and following (purple) infusion. Represented are individual replicates (dots) and mean ± SEM (bars). (**C-E**) Five minutes following the infusion, blood succinate enters in to and is metabolized by retina (n=3), cerebellum

(n=3), eyecup (n=3), liver (n=4), lung (n=3), BAT (n=3), WAT (n=3), and blood (n=7). (**C**) m+4 succinate concentration within tissues shows differential tissue entry. (**D**) Fractional labeling of m+4 succinate shows relative replacement of the succinate pool by labeled substrate five minutes following the infusion, and (**E**) $^{13}C/^{12}C$ is a ratio that in each tissue represents relative extents to which the metabolites we measure (any of which could be a product of ^{13}C-succinate; **Table 2**) are labeled by ^{13}C, relative to total ^{13}C abundance in that tissue. (**F**) Contains a representation of succinate's position in the Krebs cycle and which carbons should be labeled (purple filled circles) by metabolism of infused U-^{13}C succinate, as opposed to unlabeled carbons (purple-rimmed unfilled circles). The abundance of ^{13}C-labeled metabolites downstream of succinate (m+4 fumarate (**G**), m+4 malate (**H**), m+4 citrate (**I**), m+4 aspartate (**J**), and m+3 pyruvate (**K**)) relative to tissue m+4 succinate is respectively represented. Individual data points are represented in panels C-K, with a red horizontal line with error bars reporting the mean ± SEM.

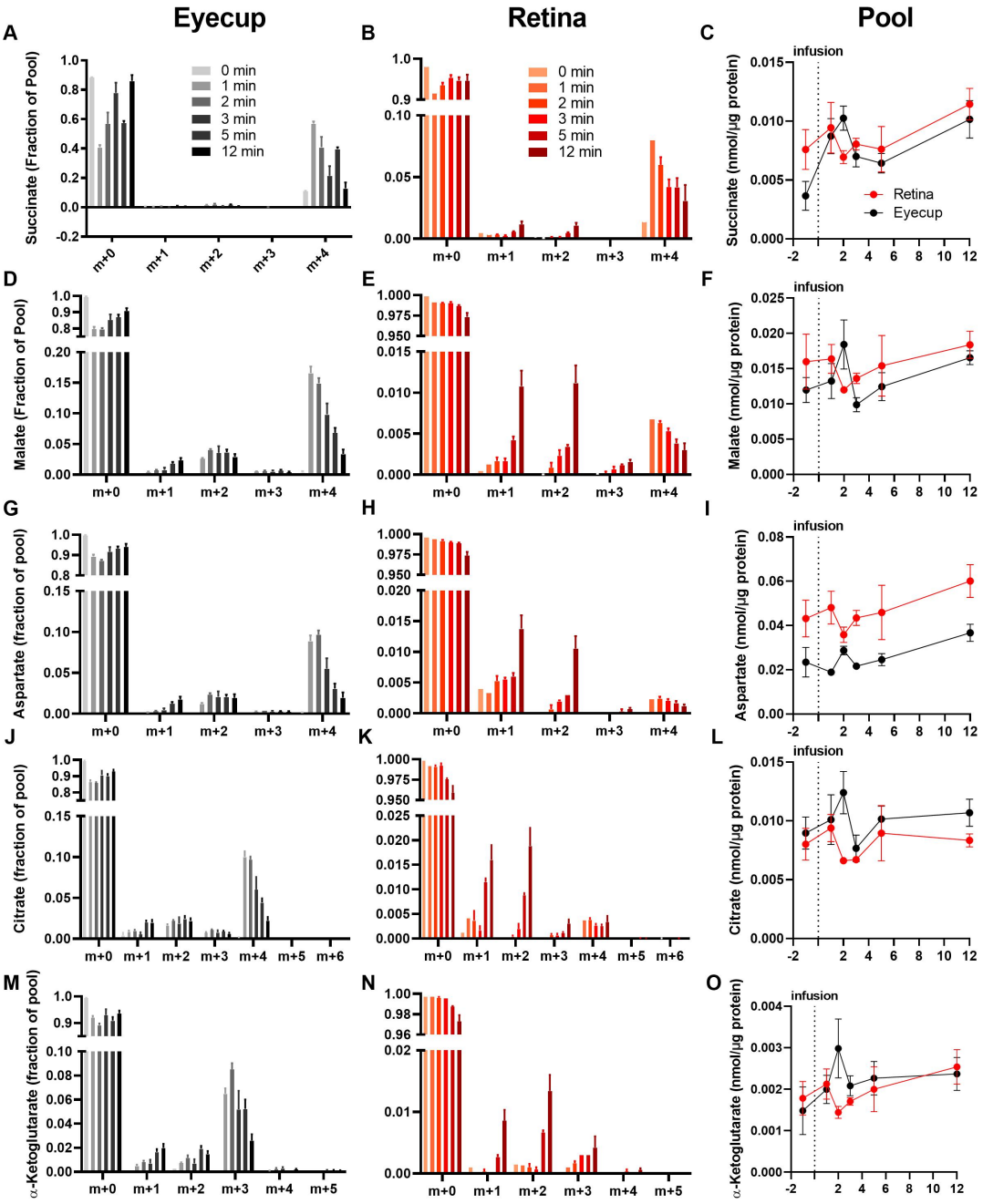

Figure 3. Infused Succinate Reveals Diverse Metabolic Routes in the Retina and Eyecup. Following bloodstream infusion of U-^{13}C-succinate in retina and eyecup, we determined the fractional labeling (**A-B, D-E, G-H, M-N**) and total abundance (metabolite pool size; **C, F, I, L, O**) of succinate (**A-C**), malate (**D-F**), aspartate (**G-I**), citrate (**J-L**), and α-ketoglutarate (**M-O**) 1, 2, 3, 5, and 12 minutes post-infusion. We compared these to labeling of tissue from un-infused catheterized C57BL6/J mice ("0 minutes"). M+*x* indicates that the molecule is ^{13}C-labeled with *x* carbons, all originating from infused succinate. N=3 for all time points except 12 minutes post-infusion, where n=6. All bars and dots represent mean ± SEM.

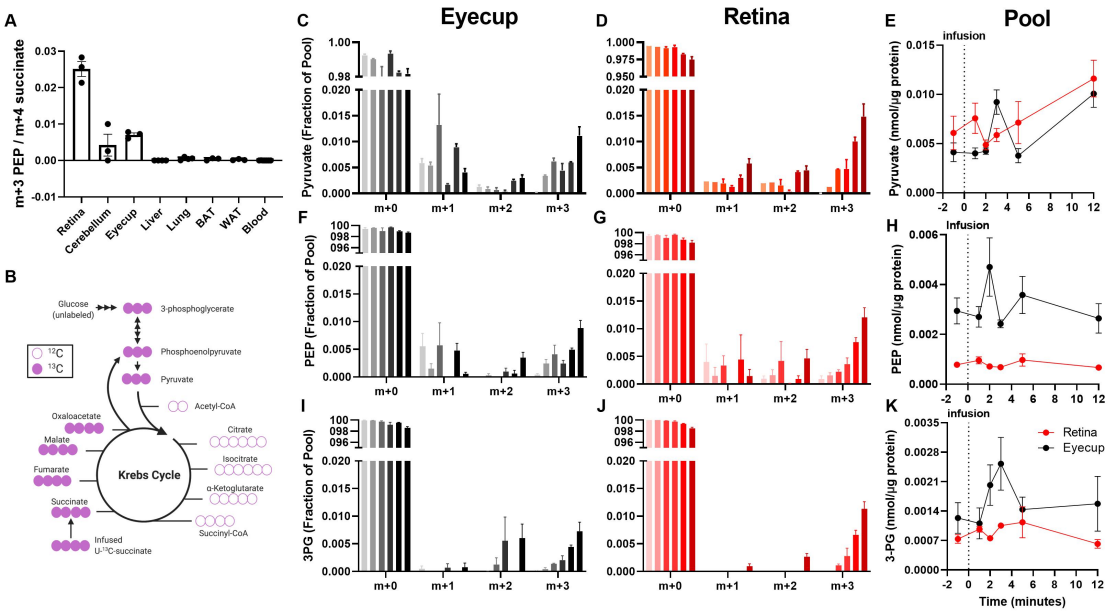

Figure 4. Infused Succinate Is Utilized to Make Glycolytic Precursors in Retina and Eyecup Tissue. (A) We determined m+3 phosphoenolpyruvate / m+4 succinate in our tissue panel 5 minutes following infusion, displaying data as in Figure 2G-K, **(B)** Schematic of the metabolic route by which ^{13}C-succinate is most likely able to label glycolytic intermediates**. (C-K)** We performed the same analysis as in Figure 3 on pyruvate (**C-E**), phosphoenolpyruvate (PEP; **F-H**), and 3-phosphoglycerate (3-PG; **I-K**). We compared these to labeling of tissue from un-infused catheterized C57BL6/J mice ("0 minutes"). M+*x* indicates that the molecule is ^{13}C-labeled with *x* carbons, all originating from infused succinate. N=3 for all time points except 12 minutes post-infusion, where n=6. All bars and dots represent mean ± SEM.

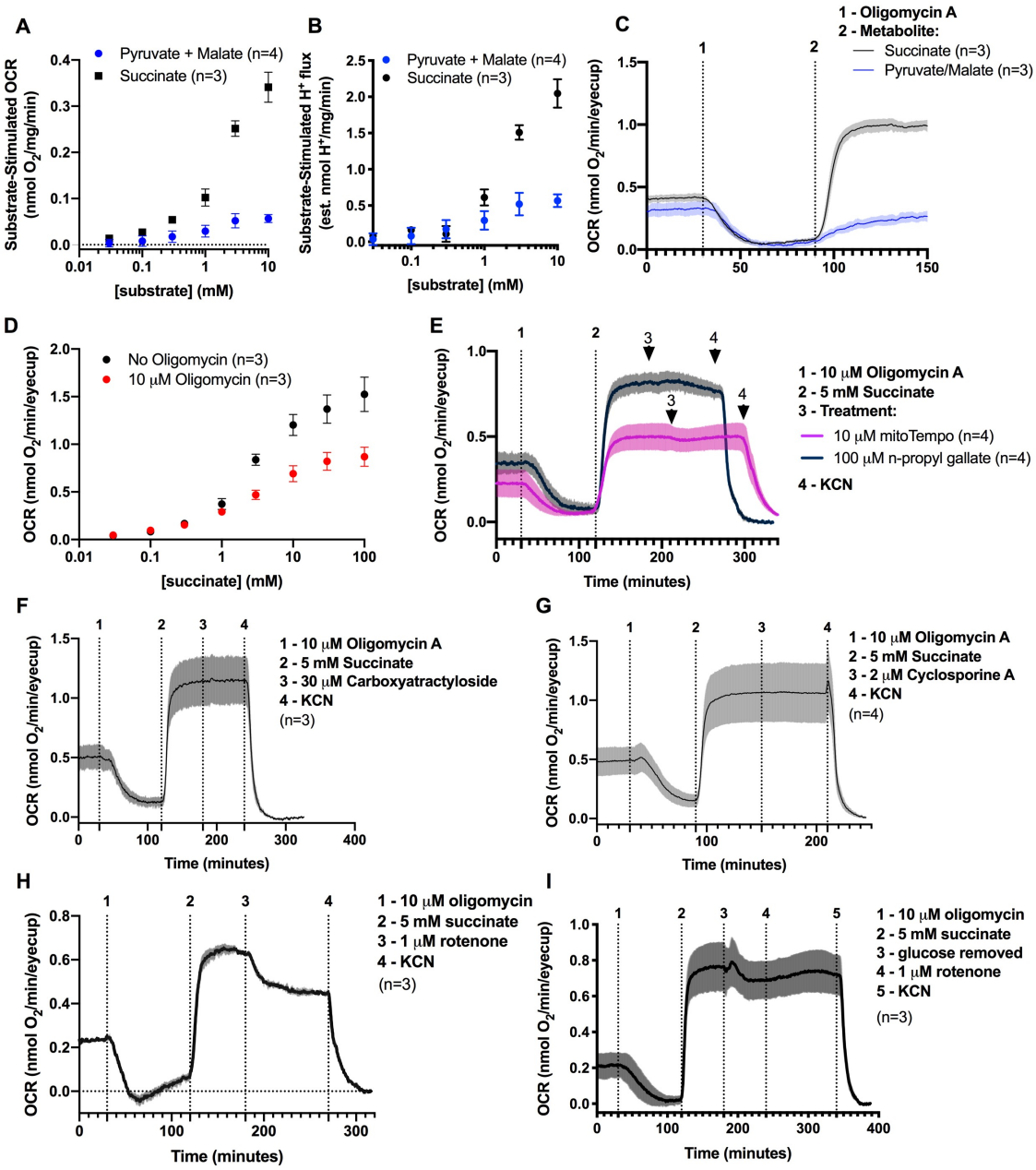

Figure 5. Extracellular Succinate Uncouples Eyecup Mitochondria *Ex Vivo*. (A) *Ex vivo* eyecup OCR as a function of substrate concentration in eyecups respiring using 5 mM glucose supplemented with increasing concentrations (30 μM, 100 μM, 300 μM, 1 mM, 3 mM, 10 mM) of succinate or equimolar malate and pyruvate. (**B**) We estimated mitochondrial H^+ flux from the matrix to the intermembrane space by multiplying OCR by the $H^+/2e^-$ ratio for the pyruvate/malate-linked substrate NADH (10) or succinate (6) (Hinkle et al., 1991). The disagreement in substrate-dependent H^+ flux between these curves suggests that additional H^+ flux in the succinate treatment is used to counter an additional H^+ conductance from the intermembrane space, suggesting that with succinate there is an H^+ conductance that is not from ATP-synthase activity. (**C**) We determined ATP-synthase-immune succinate or pyruvate/malate oxidation by incubating eyecup tissue first in 5 mM glucose, next in 5 mM glucose with 10 μM of the ATP-synthase inhibitor oligomycin A, and finally in a mix of 5 mM glucose, 10 μM oligomycin,

and 5 mM of either succinate (black) or pyruvate/malate (blue). (**D**) Succinate exhibited substantial oligomycin-resistant respiration, and we determined how much respiration is oligomycin-immune as a function of [succinate], comparing this data to Figure 1G, converted to OCR per tissue unit rather than per unit mass. (**E-I**) To determine the source of this oligomycin-resistant respiration, we performed the experimental treatments described in (C), but following the addition of 5 mM succinate to increase respiration we attempted to shut down this increase by adding (**F**) the antioxidants mito-tempo (purple line) or n-propyl gallate (black line), the adenine nucleotide translocator inhibitor carboxyatractyloside (CATR), (**G**) the mitochondrial permeability transition pore complex inhibitor cyclosporine A (CsA), (**H**) the mitochondrial complex I inhibitor rotenone, (**I**) or by removing glucose then adding rotenone. Lines represent mean O_2 consumption rate following subtraction of the 5 mM glucose "baseline" (**A,B,D**) or the 3 mM KCN "floor" (**C,E-I**).

Table 1. Best-Fit Kinetic Parameters for *ex vivo* Succinate oxidation
Least squares fit, Parameters are represented as [mean (95% Confidence Interval)]

Tissue	Basal OCR (nmol O_2 / mg / min)[&]	V_{max} (nmol O_2 / mg / min)	$K_{1/2}$ [succinate] (mM)	H*	R^2	n
Retina	0.31 (0.12-0.50)	0.12 (?**)	8.89 (1.06-?**)	0.42 (0.19-0.77)	0.81	4
Cerebellum	0.22 (0.07-0.37)	0.36 (0.31-0.42)	2.72 (1.67-4.94)	1.38 (0.81-2.73)	0.90	3
Eyecup	0.15 (0.06-0.24)	0.34 (0.28-0.46)	2.49 (1.33-8.31)	1.05 (0.55-2.24)	0.81	5
Liver	0.07 (-0.32-0.46)	0.89 (0.77-1.04)	0.90 (0.49-1.75)	1.40 (0.72-?**)	0.85	3
BAT	0.21 (0.12-0.30)	0.57 (0.51-0.66)	1.45 (0.9-2.58)	1.15 (0.72-2.04)	0.91	3
Kidney	0.48 (0.38-0.58)	0.66 (0.52-1.20)	1.50 (0.84-8.53)	1.21 (0.64-2.35)	0.88	4

* Hill's Slope
** "?" indicates that the curve fit is unable to estimate this parameter

Table 2. Metabolites used to determine total ^{13}C labeling

Metabolic process	Metabolite Name	# carbons
Glycolysis	Dihydroxyacetone phosphate	3
Glycolysis	3-phosphoglycerate	3
Glycolysis	Phosphoenolpyruvate	3
Glycolysis	Pyruvate	3
Krebs Cycle	Citrate	6
Krebs Cycle	Isocitrate	6
Krebs Cycle	α-ketoglutarate	5
Krebs Cycle	fumarate	4
Krebs Cycle	malate	4
Krebs Cycle (anapleurotic)	aspartate	4
Krebs Cycle (anapleurotic)	glutamate	5

*Although we routinely measure succinate, it was not included on this table because ^{13}C labeling on succinate could be indicative of residual infusate in the cytosol or blood-vessels.

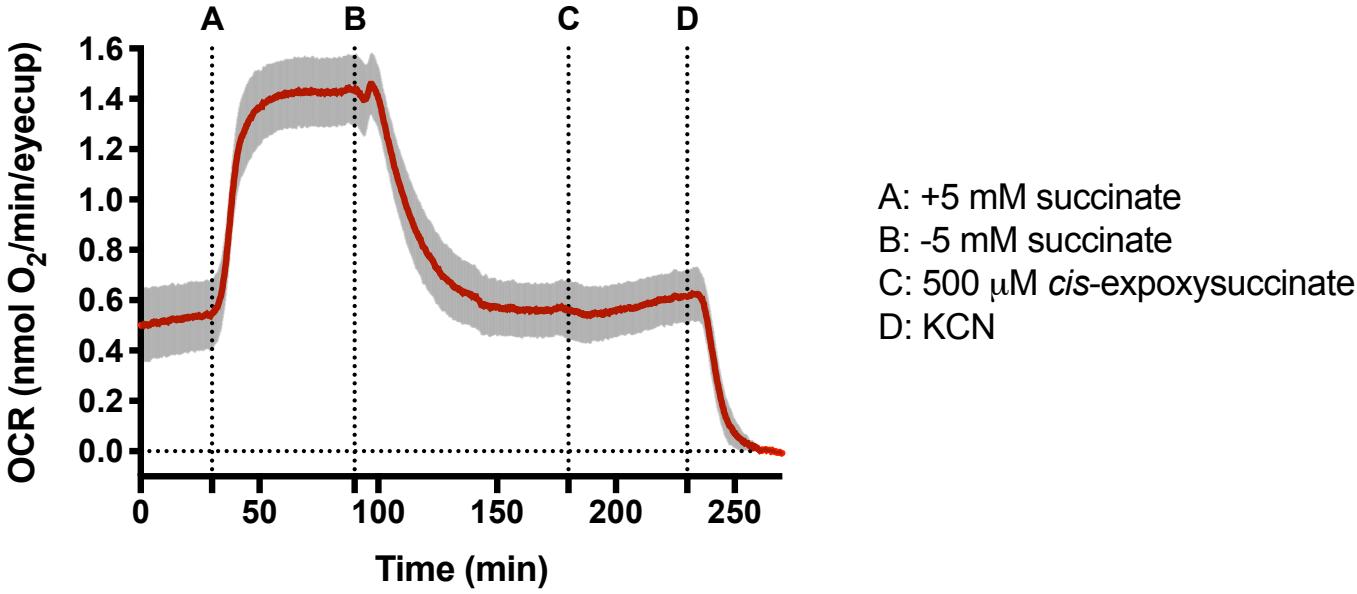

Figure S1. SUCNR1 Agonism is insufficient to increase oxygen consumption. Eyecup tissue was dissected from C57BL6J mice and ex vivo oxygen consumption rate (OCR, mean±SEM) measured as described in the materials and methods section. At baseline (0-30 minutes) the only source of energy to eyecups to fuel OCR was 5 mM glucose. At time=30 (A) minutes 5 mM succinate was added, which increased OCR ~3-fold. Succinate was withdrawn (B) and OCR fell to control values. *Cis*-epoxysuccinate is a SUCNR1 agonist with 10x greater potency for the GPCR than succinate (Geubelle et al., 2017). (C) We added 500 μM cis-epoxysuccinate to the 5 mM glucose treatment to determine whether any increases in OCR were due to metabolic changes transduced by SUCNR1. (D) KCN was used to inhibit mitochondrial complex IV OCR activity to confirm that the OCR observed in this experiment was primarally mitochondrial. We did not find any immediate effects of SUCNR1 agonism on OCR that were comparable to those of succinate itself, suggesting that succinate-induced OCR occurs mainly through direct succinate oxidation and not downstream protein signaling. (n=4)

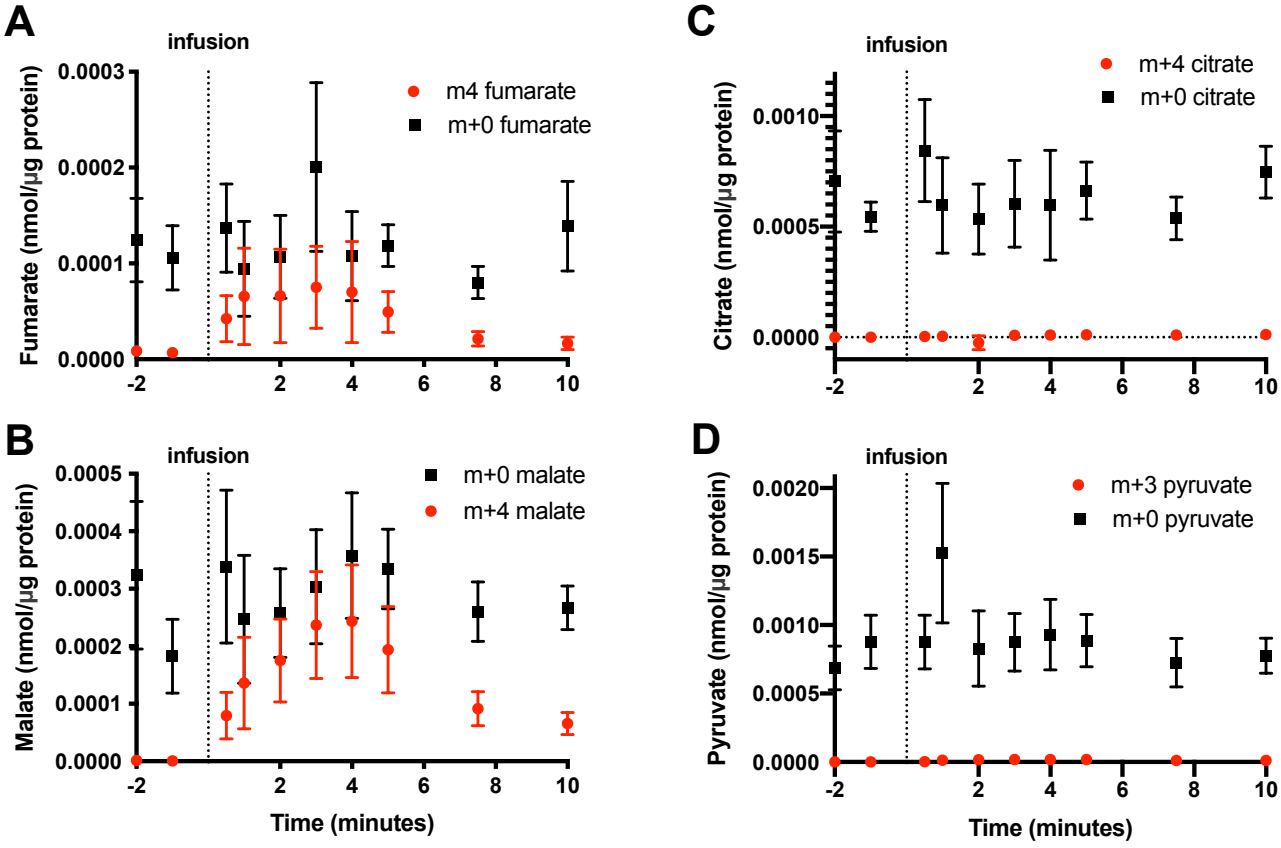

Figure S2. Post-Infusion blood Metabolite Labeling. U-^{13}C-succinate was infused into blood through a veinous catheter and 10 µL blood samples were drawn at 0.5, 1, 2, 3, 4, 5, 7.5, and 10 minutes post-infusion. Analysis of blood samples shows that following the infusion, succinate does turn over in whole blood to become (A) m+4 fumarate and (B) m+4 malate, while downstream (C) m+4 citrate and upstream (D) m+3 pyruvate appear relatively unperturbed, though this occurs to a far lesser extent than m+4 succinate turnover in blood, suggesting that rather than blood succinate feeding blood fumarate or malate pools, it is taken up into tissues. The formation of m+4 intermediates in blood does not appear to perturb the m+0 pools of unlabeled metabolic intermediates also in blood. (n=5-7)

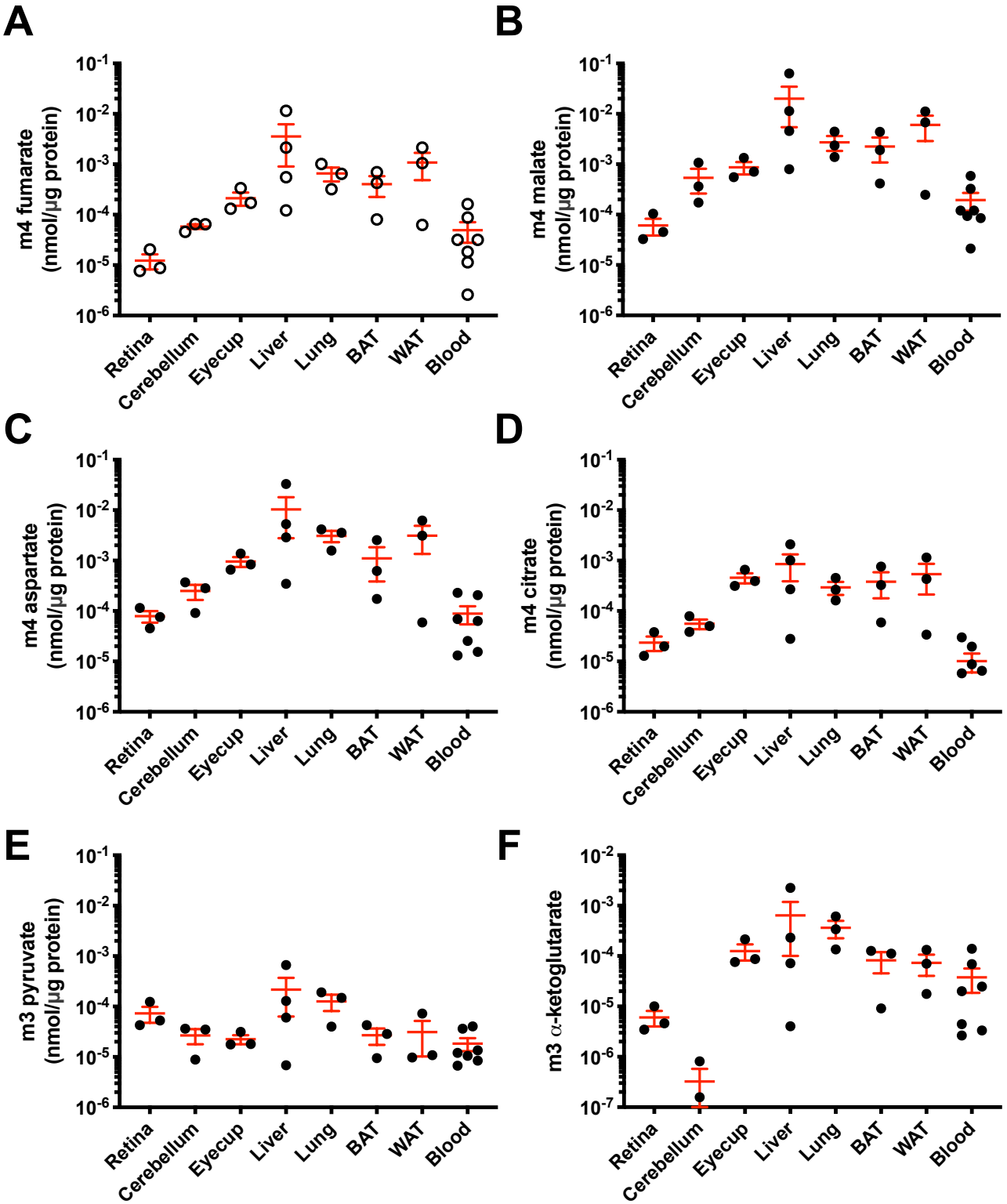

Figure S3. Abundance of labeled TCA cycle intermediates in various tissues 5 minutes following bloodstream succinate infusion. (A) m+4 fumarate, (B) m+4 malate, (C) m+4 aspartate, (D) m+4 citrate, (E) m+3 pyruvate, (F) and m+3 α–Ketoglutarate in retina, cerebellum, eyecup, liver, lung, BAT, WAT, and blood tissue. The labeling patterns of most downstream metabolic intermediates are subject to the amount of m+4 succinate imported into that tissue and thus the relative abundances of m+4 labeled matabolites closely matches that of m+4 succinate in tissues (n=3-4).

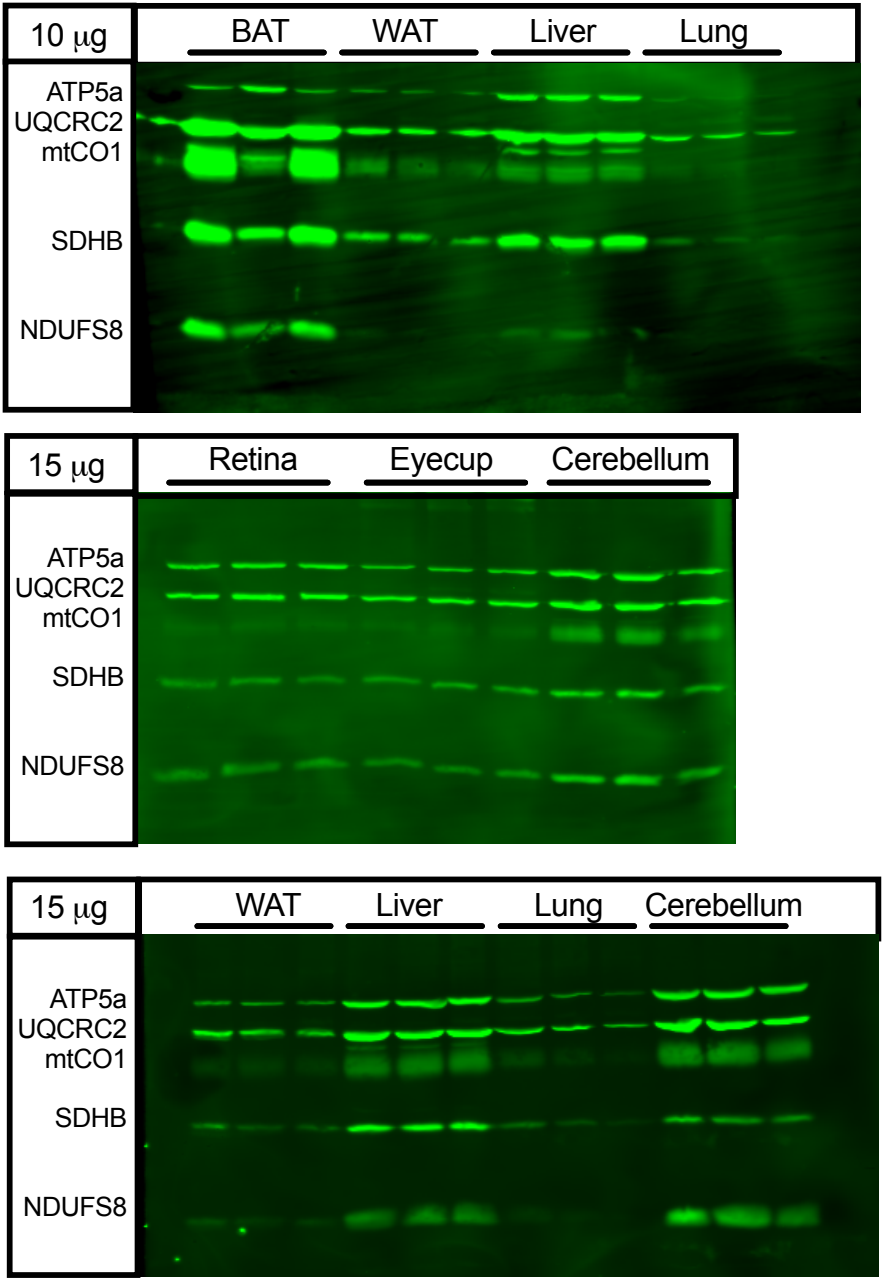

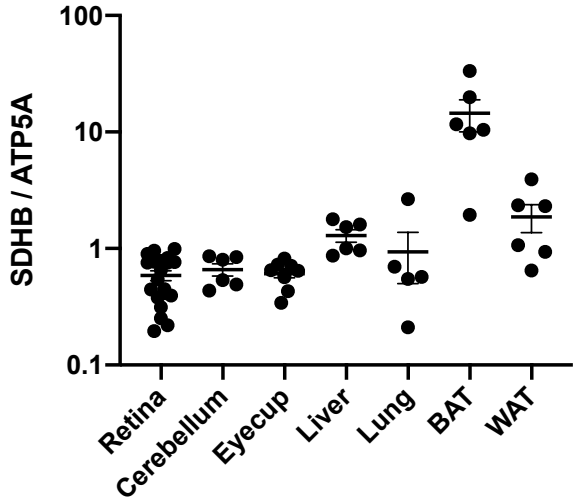

Figure S4. Mouse Succinate Dehydrogenase subunit B (SDHB) expression in a Panel of Tissues. Indicated tissues were dissected from young (~8 week old) C57BL6/J mice and lysed in RIPA buffer by sonication. Indicated protein amounts (top left corner of each blot) were loaded into and run on a 13% polyacrylamide gel, and transferred to a PVDF membrane prior to blocking and immunolabeling using a mouse anti-Total OXPHOS antibody (abcam, ab110413, diluted 1:1000). To determine mitochondrial SDHB levels, we normalized SDHB levels to those of the ATP synthase subunit ATP5a and plotted noramlized SDHB/ATP5a values for retina, cerebellum, eyecup, liver, lung, BAT, and WAT obtained across multiple blots. Mean±SEM, n=5-20, 1 outlying lung sample was excluded from this data.

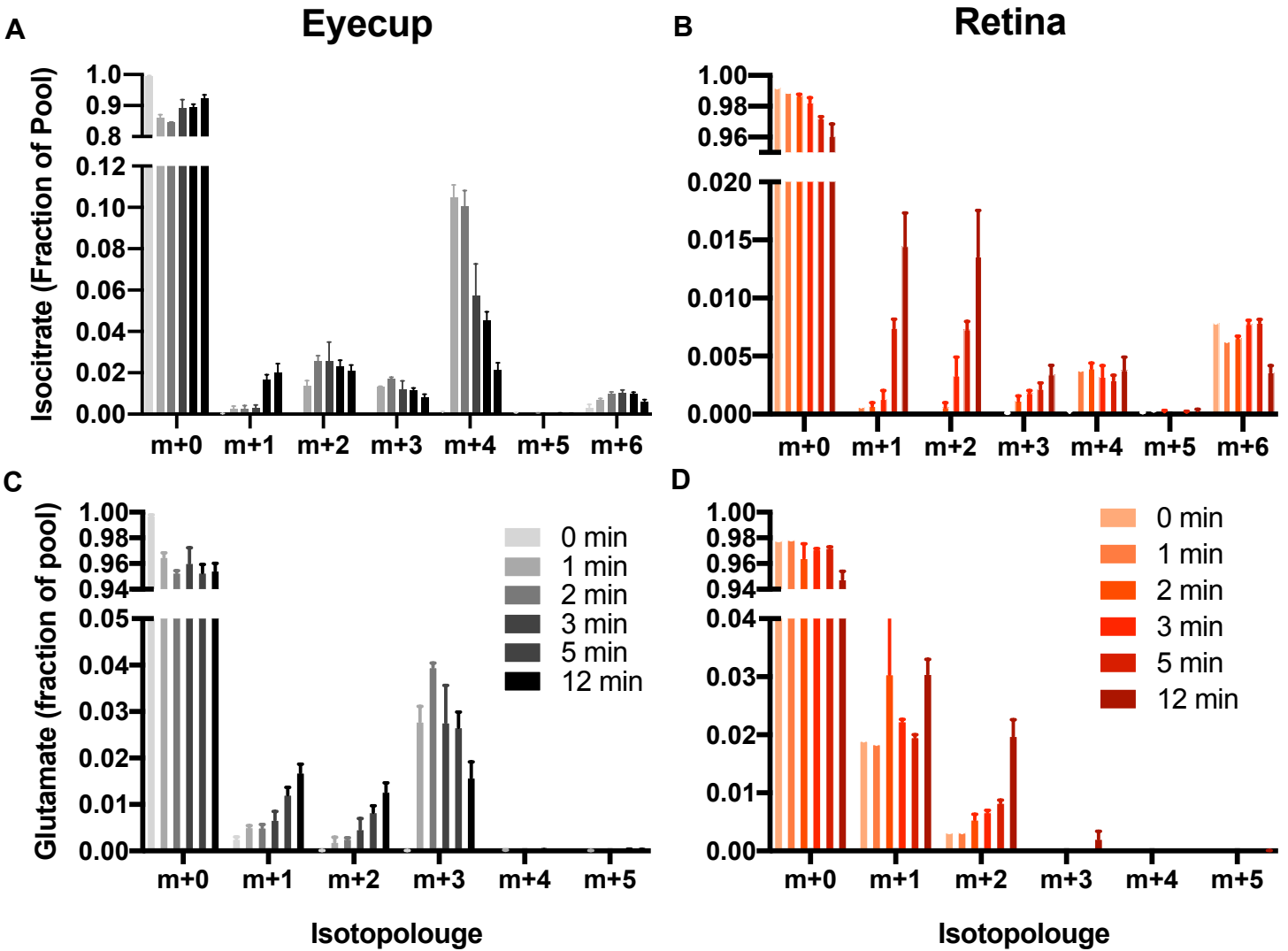

Figure S5. Isocitrate and Glutamate Isotopolouge Distributions in Retina and Eyecup Tissue Following *In Vivo* U-^{13}C-Succinate Infusion.

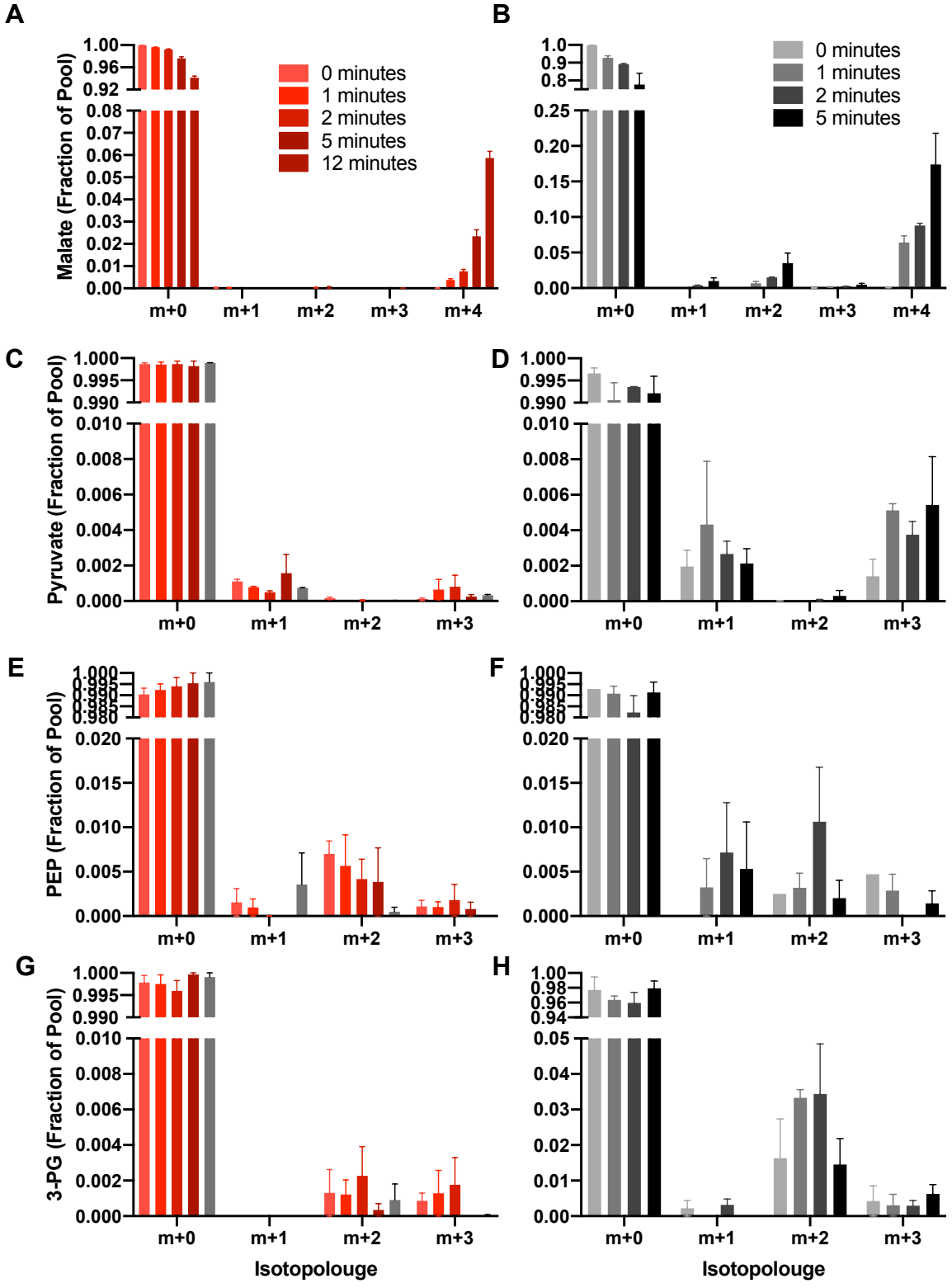

Figure S6. Lack of Gluconeogenesis in *Ex Vivo* Retina and Eyecup Tissue. Retina and Eyecup tissue was dissected from C57BL6/J mice in Hanks buffered salt solution. The tissue was next incubated in a Krebs-Ringer Bicarbonate Buffer supplemented with 5 mM glucose and 50 μM U-^{13}C-succinate equillibrated to 37°C at 5% CO_2 (n=1-3). Tissues were incubated in this buffer for 0, 1, 2, or 5 minutes and flash-frozen in liquid N_2. Tissue was homogenized, derivitized, and metabolite abundance determined using gas chromatography-mass spectrometry. Relative isotopolouge abundance was determined and is plotted for (A-B) malate, (C-D) pyruvate, (E-F) PEP, and (G-H) 3-PG. While carbons from labeled succinate do appear on Krebs cycle intermediates in both tissues (A-B) , they do not appear to accumulate m+3 labeling on Pyruvate, PEP, or 3-PG (C-H) linerarly over time as they do in vivo (Figure 4).